Journal of Materials Processing Technology 160 (2005) 278–288

Journal of Materials Processing Technology

www.elsevier.com/locate/jmatprotec

Surface roughness of a hot-dipped galvanized sheet steel as a function of deformation mode

C.M. Wichern[a], B.C. De Cooman[b], C.J. Van Tyne[c,*]

[a] *Max-Planck-Institut für Eisenforschung GmbH, Max-Planck-Straße. 1, Düsseldorf 40237, Germany*
[b] *Laboratory for Iron and Steelmaking, Vakgroep Metallurgie en Materiaalkunde, Universiteit Gent, Technologiepark 9, B-9052 Zwijnaarde, Belgium*
[c] *Department of Metallurgical and Materials Engineering, Colorado School of Mines, Golden, CO 80401, USA*

Received 12 February 2003; received in revised form 17 June 2004; accepted 17 June 2004

Abstract

A hot-dipped galvanized zinc-coated sheet steel was deformed with three different laboratory test systems: a Marciniak punch system, a flat-die friction test system, and a cupping system. These systems were able to impose various combinations of deformation modes to the sheet. The deformation modes include: (1) strain without die contact, (2) sliding, (3) pressing, and (4) bending. Strain measurements from the electrolitically gridded specimens were made at the same locations as surface profilometry measurements, allowing a direct correspondence of surface roughness with strain. Quantification of the roughening as a function of strain, sliding and bending was determined. The roughening rate depends upon the strain level as well as the strain path. Increased strain without die contact causes an increase in the surface roughness with strain paths close to plane strain exhibiting the highest roughening rate. The deformation modes of sliding, pressing, and bending cause a decrease in the surface roughness (i.e. smoothing) to occur. A first-order model is proposed to account for the surface roughness as a function of these deformation modes.

Keywords: Surface roughness; Electron beam textured sheet; Strain without die contact; Sliding; Pressing; Bending

1. Introduction

Complex forming operations are often used to shape coated sheet steels into many products. During these operations, the deformation imparted to the zinc-coated surface can be classified into four distinct modes: (1) strain without die contact, (2) sliding, (3) pressing, and (4) bending. The condition of the zinc-coated surface after these types of deformations must be monitored separately from the substrate, because the zinc coating may not necessarily have the same forming behavior as the sheet steel. The zinc-coated surface may develop defects, such as unacceptable roughening, cracking or powdering, as a result of a forming operation even though the sheet steel itself performs well [1].

The purpose of the present work is to quantify the effect of different deformation modes on the changes that occur to the zinc-coated surface. Such relationships would be useful in assessing the effect that various forming operations have on the subsequent surface quality of the final part. These relationships are developed by measuring both the deformation applied to the sheet steel and the resulting surface topography of the zinc coating in a manner that allows direct correlation of the measurements.

2. Background and theory

2.1. Strain without die contact

The level of strain imparted to a sheet will affect its mechanical properties, including strength, toughness, anisotropy, microstructure, and many others. These properties play

* Corresponding author. Tel.: +1 303 273 3793; fax: +1 303 273 3795.
E-mail address: cvantyne@mines.edu (C.J.V. Tyne).

0924-0136/$ – see front matter © 2004 Elsevier B.V. All rights reserved.
doi:10.1016/j.jmatprotec.2004.06.017

a role in the formability of the sheet, and can affect the material either locally or on a bulk scale [2]. The mechanism by which the material fails is dependent on these material properties, as well as the strain path, which also has an effect on sheet steel forming [3].

The strain level, as quantified by the VonMises equivalent strain [4] and grain size, are cited in the literature as being the most important factors affecting the surface roughening during deformation [5,6]. For a plastically deformed material, the VonMises equivalent strain is

$$\varepsilon_{\text{vme}} = \sqrt{\tfrac{4}{3}(\varepsilon_1^2 + \varepsilon_2^2 + \varepsilon_1\varepsilon_2)} \quad (1)$$

where ε_1, ε_2 and ε_3 are principal strain components and that volume constancy occurs during plasticity, $\varepsilon_1 + \varepsilon_2 + \varepsilon_3 = 0$. It should be noted that the ε_{vme} value gives no indication of strain path, which for sheet deformation is often characterized by the ratio of the principal strain components, ε_1 to ε_2. The Keeler–Goodwin [7] forming limit diagram (FLD), Fig. 1, quantifies strain path effects using the major and minor strains in the plane of a deformed sheet, to describe the reaction of the sheet to applied deformation. Fig. 1 shows three general strain paths that are referred to as drawing (left side of FLD), plane strain ($\varepsilon_{\text{minor}} = 0$) and stretching (right side of FLD).

2.2. Sliding

Deformation by sliding occurs when the sheet is forced to slide along a die surface, and may occur with or without strain. For example, in a flat-die friction test, the sheet slides between two dies but does not experience any significant elongation strain. But in a deep drawing or cupping process, the flange region of the sheet slides between the lower die and blank holder. The sheet in this operation is also being compressed in the radial direction as it moves toward the die shoulder.

2.3. Pressing and bending

During sliding deformation, there is often a simultaneous normal pressure imposed upon the sheet. In the present work, we have not completely separated the roughness changes due to sliding from the roughness changes due to pressing; therefore, the quantification of the pressing pressure has not been attempted. We do propose that the pressing mode of deformation be considered as a separate entity in the extension of the first-order model that is developed herein.

Bending is imposed on the sheet during a cupping operation, as the sheet is pulled over the die shoulder. On the inner side of the bend, the sheet will experience compressive strains and on the outer side of the bend, tensile strains will be imposed. We have not attempted in this work to quantify the strain that occurs during the bending operation.

2.4. Three-dimensional surface topography analysis

In order to examine the effects of forming on the surface of the workpiece, some quantitative measure must be used. There are a large number of roughness parameters that can be used to describe various aspects of a surface. From these parameters the root mean square average roughness parameter, S_q, was chosen for its basic nature and widespread usage [8]. The parameter is calculated as:

$$S_q = \sqrt{\frac{1}{MN}\sum_{j=1}^{N}\sum_{i=1}^{M}\eta^2(x_i, y_j)} \quad (2)$$

where M and N are the discretized surface matrix size, and η is the height at surface coordinates x and y.

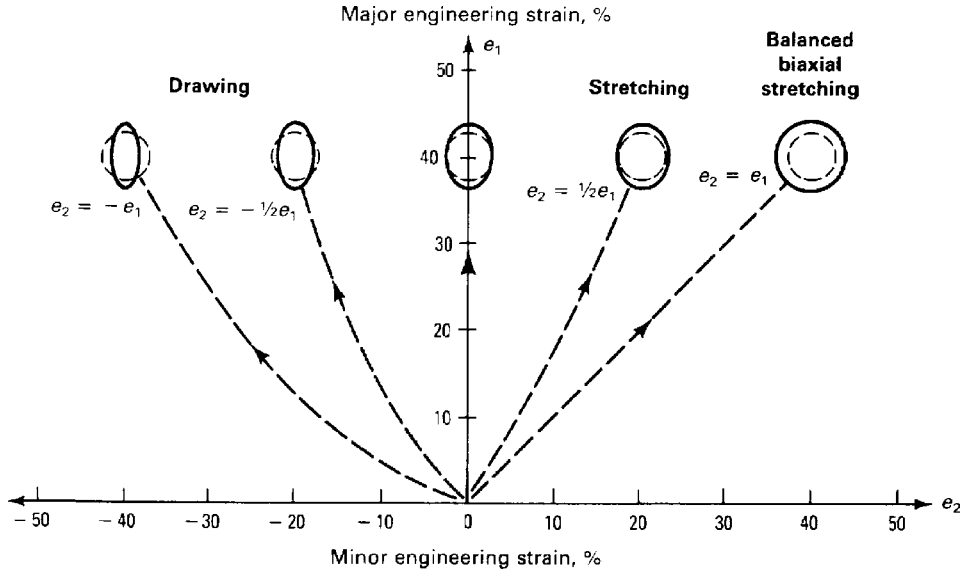

Fig. 1. Plot of major engineering strain vs. minor engineering strain for five different strain paths ranging from drawing to biaxial stretching [7].

3. Experimental methods

3.1. Materials

The experimental testing was performed on an interstitial free (IF) steel substrate with a hot-dip galvanized (HDG) coating. During production, two separate surface textures (EBT — electron beam textured roll) were imparted onto the material. The final cold roll in the tandem mill before the coating process imparted an EBT texture with ring diameters, ϕ, 100–150 μm, a minor lateral spacing, d_l, of 225 μm and a major lateral spacing, d_q, of 388 μm. After the zinc coating, the EBT textured rolls of the temper mill imparted a second EBT-type roughness onto the surface of the zinc coating. The EBT texture parameters were ϕ = 170–180 μm, d_l = 318 μm and d_q = 550 μm. For both surface-texturing operations, one side of the sheet d_l is parallel to the rolling direction and d_q is perpendicular to the rolling direction and on the other side of the sheet d_q is parallel to the rolling direction and d_l perpendicular. The depths of the features imparted by the textured rolls are on the order of 20 μm, which is an order of magnitude greater than the surface roughness of the coating. Fig. 2a shows the coated surface resulting from the final skin pass texturing, which is the topography of the HDG

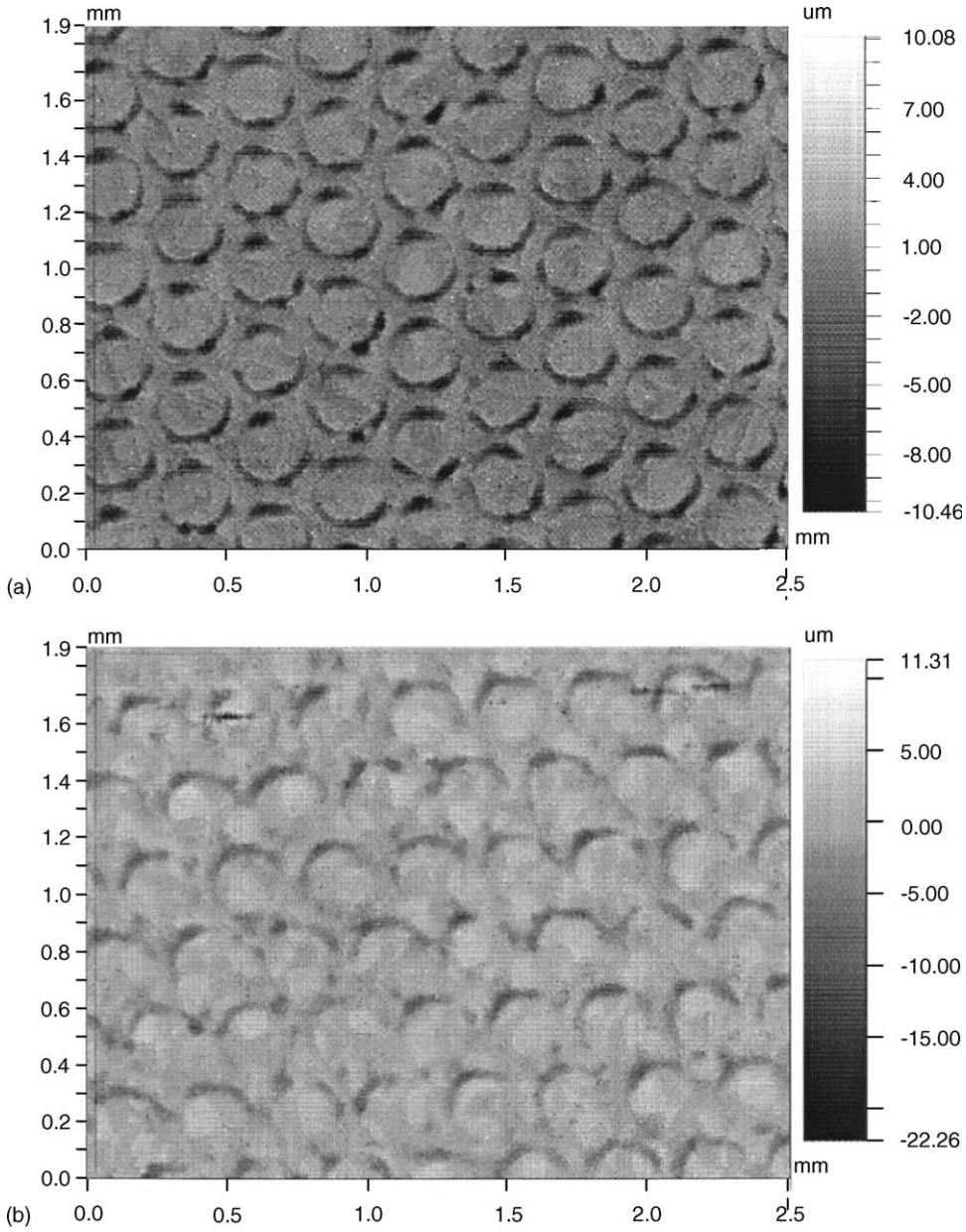

Fig. 2. (a) Initial surface topography of HDG zinc-coated sheet steel with EBT surface pattern. The gray scale to the right of the image is the height of the individual points in the image. The height scale units are microns. (b) Surface topography of IF steel substrate after removal of the zinc coating. Two EBT surface patterns can be seen. The gray scale to the right of the image is the height of the individual points in the image. The height scale units are microns.

material in the untested condition. Fig. 2b shows the topography of the substrate material after the coating has been removed, which upon examination shows both the large and small EBT texture pattern.

3.2. Laboratory mechanical tests

Different forming modes were imparted to the coated sheet steel via several laboratory mechanical tests. The mechanical testing consisted of three different types: Marciniack punch tests, flat-die friction tests, and cup tests. After testing, the surface topographies from each of these tests were measured via three-dimensional surface profilometry, and the strains imparted during Marciniack punch and cup testing were measured via square grid analysis. The strain measurements and the surface profilometry measurements were performed at the same position on the specimen. This enabled a direct correlation between deformation and surface topography.

3.3. Marciniack punch testing

Strain deformation without die contact was imparted to the sheet by Marciniak tests performed to four different punch depths (15, 25, 35 mm and to failure) along eight different strain paths. These eight strain paths were realized through the use of test specimens with different widths. The lengths of all specimens used for the current work were 300 mm, and the widths were 60, 120, 150, 180, 200, 220, 230, and 300 mm. The 60 mm wide specimen corresponds to a drawing strain path, the 180 mm wide specimen corresponds to the plane-strain strain path, and the 300 mm wide specimen corresponds to a biaxial stretching strain path. The drawbead force used during testing was increased until no slippage occurred through the locking drawbeads. Spacer sheets of 300 mm × 300 mm with a circular hole in the center were used during testing to eliminate the effects of friction that would be applied to the test specimen via the face of the Marciniack punch. Fig. 3 shows the geometry of this test configuration. After deformation via Marciniack punch testing, strain analysis and surface profilometry were performed on each tested specimen.

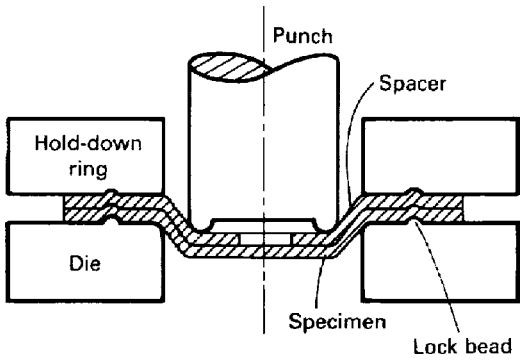

Fig. 3. Schematic diagram of Marciniack punch test setup showing both test specimen and spacer sheet [7].

The strain analysis was performed using a pattern of square grids measuring 2.5 mm × 2.5 mm. The grid pattern was electrolytically etched onto the surface of the specimen prior to testing with one axis of the grid parallel to the longitudinal axis (i.e. the rolling direction) of the sheet and the other parallel to the transverse axis of the sheet. After testing, the change in size of the grid in both the longitudinal and transverse directions and the initial grid size were used to calculate strain imparted to the sheet. Fig. 4 shows the position of the strain measurements and the most common location for a failure.

After deformation, three-dimensional non-contact surface profilometry was performed on the surface of the tested sheets. The surface profilometer used was a Wyko

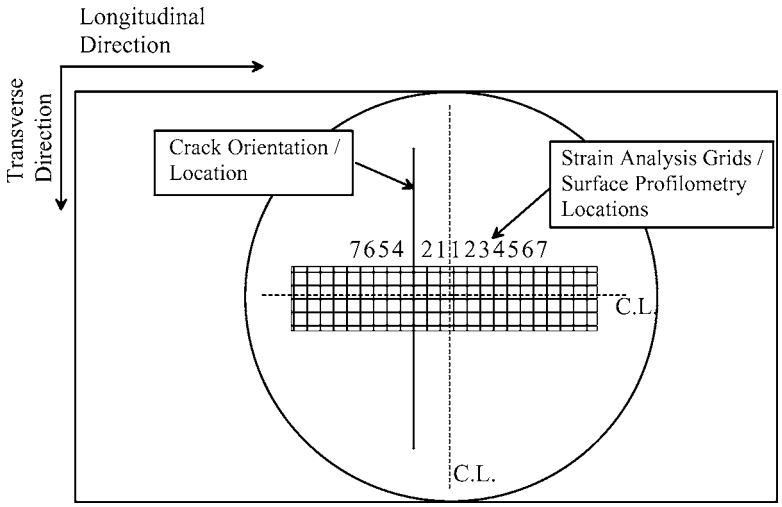

Fig. 4. Position of strain measurements and usual location of failure for Marciniack punch tested specimens. The circular region is the area deformed by the Marciniack punch. A representative region of 2.5 mm^2 grid pattern and the associated strain measurement locations are also shown.

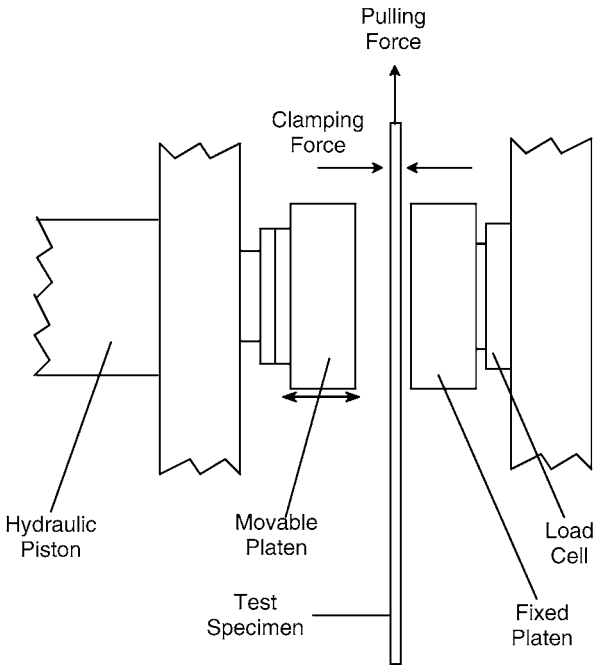

Fig. 5. Schematic diagram of flat-die friction testing apparatus.

corporation RST system. All surface scans were performed at 2.5 times magnification with a field of view of approximately 2.0 mm × 2.5 mm. At this magnification, the size of the matrix of surface heights is 236 points wide by 368 points long with a lateral resolution of approximately 7 μm. This level of lateral resolution is still well within the range necessary to capture the major features of the EBT surface, which has lateral features on the order of 100–600 μm.

3.4. Flat-die friction testing

A flat-die friction testing system was used to impart sliding deformation to the HDG material. The sliding deformation was performed using a commercial flat-die friction test system similar to the schematic in Fig. 5. Test specimens were 50 mm wide and a test length of 150 mm was used. Normal load, 5.0 kN, and sliding speed, 50 mm/s, were controlled via the software used for operating the test apparatus.

Surface profilometry was performed at each of the measured grid squares using the Wyko RST surface profilometer in the same manner as the Marciniak punch tested specimens. Surface scans were performed in center region of the test specimens. The locations of the scans were at positions of increasing sliding distances (0–45 mm in increments of 5 mm) with respect to the leading edge of the flat dies.

3.5. Cup testing

To impart sliding, pressing, and bending deformation, cup drawing tests were performed on the HDG material. Fig. 6 shows a schematic diagram of the cup forming method used to impart the desired deformation.

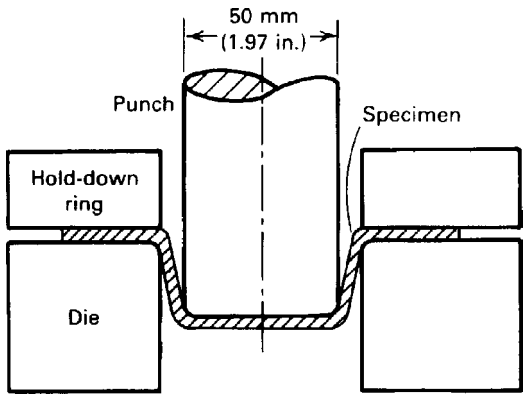

Fig. 6. Schematic diagram of cup forming apparatus used during the current work [7].

Two different types of cup testing were performed. The first was a full cupping operation. A disc with ϕ = 150 mm was deformed into a cup shape using a punch with ϕ = 50 mm. Blank holder force, 13 kN, and punch speed, 70 mm/s, were maintained constant while punch force was recorded. The second cup test was an interrupted test. The test was stopped while the flange of the specimen was still in the blank holder. This type of testing was performed using punch depths of 10, 20 and 30 mm.

All of the blanks for the cupping operations were electro-gridded with the same grid used on the Marciniack punch test specimens. Fig. 7 shows that upon completion of cupping, the strain levels imparted to the sides of the cup were measured for the full cupping operation in regions on the outside of the cup. Fig. 7 also shows the strains imparted to the flange region of the cup, measured in regions on the flange for the interrupted cupping operation.

Surface profilometry was performed in the same manner for cupped specimens as it was for the Marciniack punch deformed specimens and the flat-die friction tested specimens. Surface profiles were again taken at the same location as strain measurements to create a direct correspondence between applied deformation and surface topography.

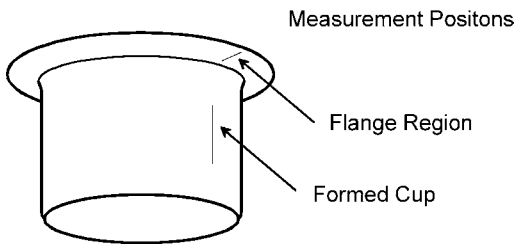

Fig. 7. Schematic of partially formed cup. The two lines indicated where both strain analysis and surface profilometry were performed.

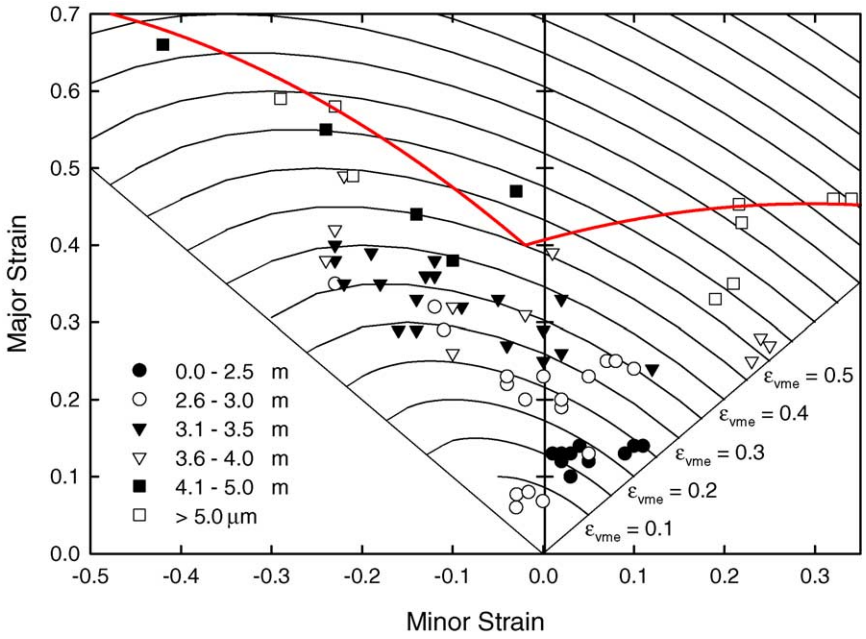

Fig. 8. Forming limit diagram for the HDG sheet steel with iso-ε_{vme} lines and roughness values for different strains.

4. Results

4.1. Marciniack punch tests

Fig. 8 shows the surface changes due to strain on the forming limit diagram for the sheet steel. This figure provides a comparison of the VonMises equivalent strain, ε_{vme}. The semi-elliptical lines on this figure are iso-ε_{vme} lines. In Fig. 8, the surface roughness, S_q, of the material surface is reported via five different levels. Each of the five levels is represented by a different symbol style. Fig. 9 is a plot of roughness versus strain, ε_{vme}, for the eight strain paths used during the Marciniak punch deformation. The roughness increases with strain.

4.2. Flat-die friction tests

The flat-die friction testing of the HDG sheet steel resulted in the relationship between sliding distance, X_{slid}, and roughness as shown in Fig. 10. As the sliding distance increased,

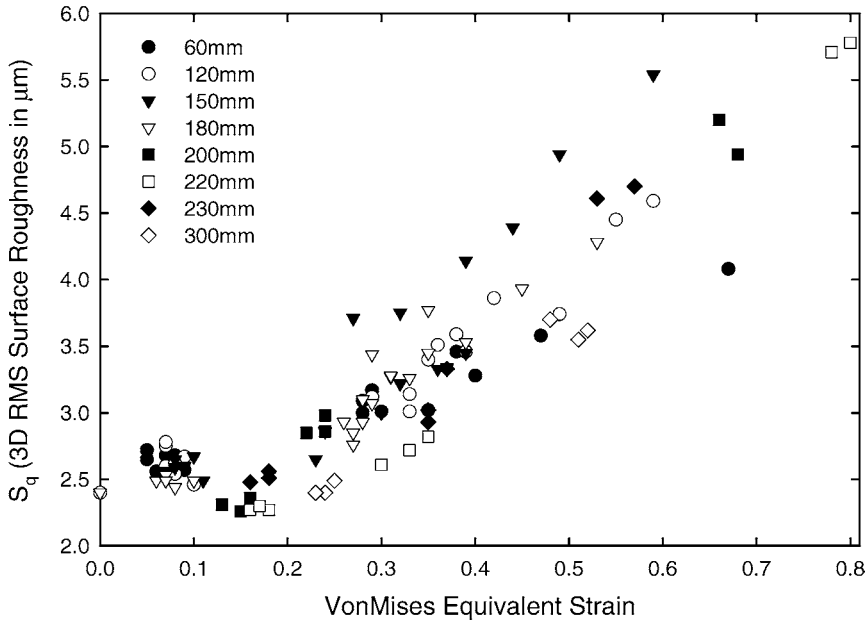

Fig. 9. Surface roughness as a function of strain for different strain paths imposed by Marciniak punch deformation.

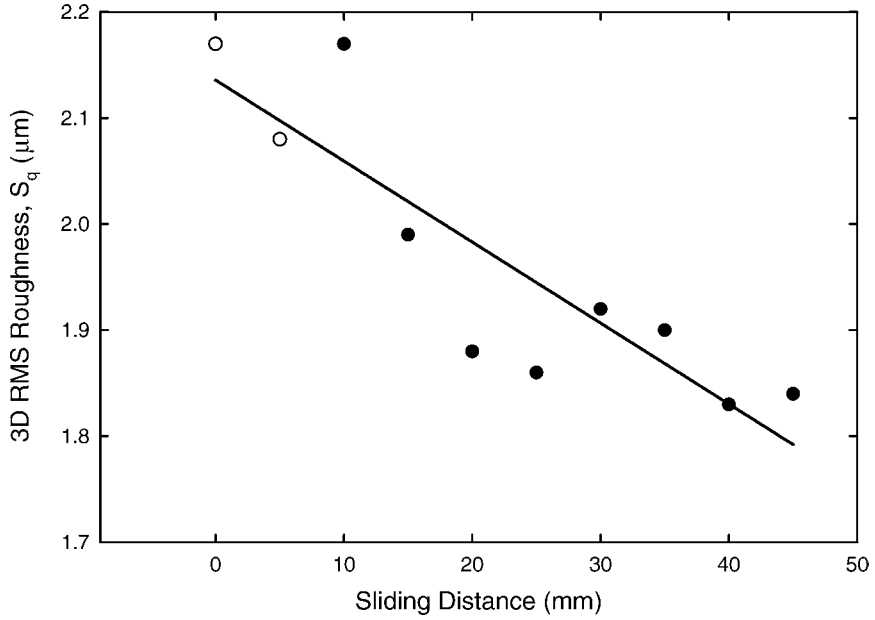

Fig. 10. Surface roughness as a function of sliding distance for HDG sheet steel tested using a flat-die friction tester.

the surface roughness decreased, indicating that the sliding mode of deformation is a smoothing process.

4.3. Cupping tests

Roughness versus strain plots were created for the cupped materials. Fig. 11 shows roughness versus strain plots for both cupping operations and the Marciniak punch deformation performed along the drawing strain path.

5. Discussion

5.1. Surface roughness and the forming limit curve

Fig. 8 reveals a relationship between the highest roughness levels and the forming limit curve. On the draw side, the highest roughness values and the forming limit curve correspond well. For strain paths that are increasingly plane strain, the roughness levels near the forming limit curve are lower.

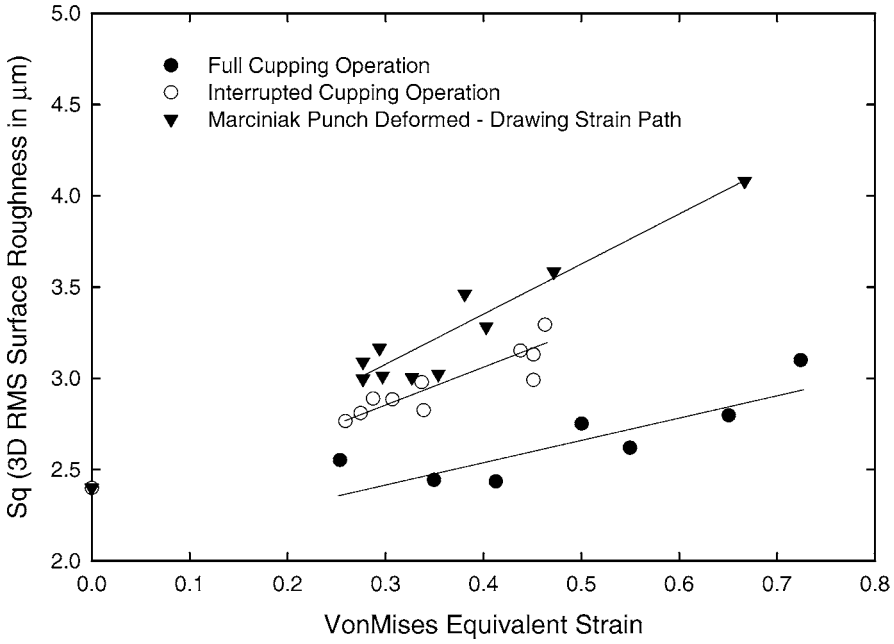

Fig. 11. Surface roughness as a function of strain for Marciniak punch deformation (drawing strain path) and cupping operations.

Table 1
Rate of roughening for different strain paths

Marciniak specimen width (mm)	$m^{\varepsilon}_{S_q}$ (μm)
Drawing	
60	3.2
120	3.9
150	4.8
Plane strain	
180	4.0
200	4.2
220	4.0
230	3.9
Biaxial stretching	
300	2.8

On the stretch side, the highest roughness levels correspond well to the forming limit curve at biaxial stretching. However, some points in the stretch region exhibit the highest roughness level well below the forming limit curve. The implication of this observation is that, although a material and a forming process might be safe according to the forming limit diagram criteria, the surface of the sheet may roughen to the point where surface quality becomes problematic.

5.2. Surface roughness and strain path

Although a general trend of increasing surface roughness, S_q, with increasing VonMises equivalent strain, ε_{vme}, is observed and shown in Fig. 8, the roughness values do not consistently match with iso-ε_{vme} lines. The lack of correspondence between the roughness and strain is somewhat contradictory to previous investigations, which found that roughness is a function of ε_{vme} and grain size, but not dependent upon strain path [5,6].

To determine the dependence of roughness on strain and strain path, S_q for the eight strain paths has been plotted as a function of ε_{vme}, in Fig. 9. Fig. 9 shows that roughness is essentially a linear function of strain for each individual strain path. The strain path dependence of roughness is related to the slopes of the lines plotted for each of the different strain paths shown in Fig. 9. These slopes are the roughening rate, $m^{\varepsilon}_{S_q}$, with respect to strain and the values are given in Table 1. The highest rates of roughening ($m^{\varepsilon}_{S_q}$ = 4.0–4.8 μm) are observed for strain paths close to plane strain. The rate of roughening ($m^{\varepsilon}_{S_q}$ = 3.2 μm) decreases as the strain path moves towards drawing or biaxial stretching which shows the lowest rate of roughening ($m^{\varepsilon}_{S_q}$ = 2.8 μm).

The observations about the roughening rate dependence on strain path provide a possible explanation for the minimum in the forming limit curve at plane strain. Marciniak and Kudzinski have explained sheet failure via the presence of a preexisting defect and strain localization [9]. The local stress state in a preexisting defect is different than the stress state in the sheet itself. The localized stresses in the defect may reach instability before the rest of the sheet, initiating the failure. A defect of critical size may occur due to increased surface roughness. Table 1 shows that a plane-strain strain path has the highest roughening rate. If the critical defect size for localization of deformation is actually a surface feature caused by roughening, the development of a critical defect can occur at the lowest strain level along the strain path with the greatest roughening rate.

A significant feature of Fig. 9 is the group of tests performed at very low strain levels. These tests do not correspond to the linearity seen for higher strain levels. Because of these data points, it appears that the zinc-coated surface roughens upon application of very low strains, smoothes out again at somewhat higher strains, and then proceeds to roughen once again continuously up to the highest strains. Surface roughness evolution of this nature is unexpected. A proposed explanation of this phenomenon is the subject of another paper [10].

5.3. Surface roughness and deformation mode

Examination of the roughness evolution during the three different deformation processes can be used to assess surface changes due to different forming modes. The specimens from the 60 mm Marciniack tests, which are subjected to strain without die contact along a drawing strain path, are replotted in Fig. 11. The specimens deformed by an interrupted cupping process are subjected to a deep drawing strain path and additionally pressurized sliding as the material moves along the blank holder. The specimens deformed by a full cupping operation are subjected to deep drawing strain, pressurized sliding and additionally bending as the test specimen moves over the die shoulder. The bending causes compression of the sheet on the outside surface of the cup as it passes over the die shoulder. Fig. 11 also plots the data from these two cupping tests.

During the Marciniak punch deformation, surface roughness increases with increasing levels of strain, as seen in Fig. 11. Results from both cupping operations shown in Fig. 11 also show an increase in roughness with an increase in strain. However, roughness data from the cupping operations are below the data from the Marciniak punch operation for the same strain values. The rate of roughening for the full cupping operation is slightly lower than the rates of roughening for the interrupted cupping operation and the Marciniak punch deformation. From Fig. 11, it can be surmised that pressing, sliding, and bending deformation modes lead to a decrease in the amount of roughening.

5.4. Proposed model

If one assumes that roughness is a linear function with respect to both strain and sliding distance, and that the strain induced roughening is the same for both Marciniak punch deformation along a drawing strain path and cupping deformation, then the effects of strain and sliding on the surface topography can be separated. For the Marciniak punch

deformation (i.e. strain without die contact) there are no sliding, pressure, or bending effects, and the relationship between roughness and strain has the linear form of:

$$S_q = S_q^0 + \varepsilon_{vme}\, m_{S_q}^{\varepsilon} \quad (3)$$

where S_q^0 is the roughness before testing and $m_{S_q}^{\varepsilon}$ is the roughening rate with respect to strain. For the interrupted cupping operation (i.e. strain and sliding under pressure) the relation for roughness can be written as:

$$S_q = S_q^0 + \varepsilon_{vme}\, m_{S_q}^{\varepsilon} + X_{Slid}\, m_{S_q}^{PX} \quad (4)$$

where X_{Slid} is the interface sliding distance and $m_{S_q}^{PX}$ is the roughening rate due to sliding under pressure. It is likely that a pressure value, P_N, should be included in the sliding term, because when no normal pressure is present, sliding should have no effect on the surface roughness. This would cause the third term in Eq. (4) to become $X_{Slid}\hat{m}_{S_q}^{PX} P_N$. It has been found that roughness varies linearly with normal pressure for constant sliding distances [11]. In the present analysis, this pressure effect is neglected.

If the effect of bending on roughening is considered to be independent with respect to strain and sliding distance – a reasonable first assumption for the full cupping tests since the material bends over the same die radius regardless of previous strain or sliding distance – then the roughening behavior for the full cupping operation can be written as:

$$S_q = S_q^0 + \varepsilon_{vme}\, m_{S_q}^{\varepsilon} + X_{Slid}\, m_{S_q}^{PX} + K_{Bend} \quad (5)$$

where K_{Bend} is a constant representing the amount of roughening attributed to bending.

The numerical value of $m_{S_q}^{\varepsilon}$ in Eq. (3) for the Marciniak punch deformation along a draw strain path can be calculated from the experimental strain and surface topography data. The value of $m_{S_q}^{\varepsilon}$ can be substituted into Eq. (4), and then Eq. (4) can be solved for $m_{S_q}^{PX}$ using the experimental strain, sliding distance and roughening data from the interrupted cupping operation. The first two rows in Table 2 present the numerical values for these parameters.

Table 2
Roughening parameters due to strain, sliding distance and bending

	$m_{S_q}^{\varepsilon}$ (μm)	$m_{S_q}^{PX}$ (μm/mm)	K_{Bend} (μm)
Marciniak punch deformation	3.2	–	–
Interrupted cupping operation	3.2[a]	-8.5×10^{-3}	–
Full cupping operation	3.2[a]	-23.0×10^{-3}	−0.10
Flat-die friction test sliding	–	-9.7×10^{-3}	–

[a] Value assumed from Marciniak test.

To test the validity of the model, the smoothing (i.e. negative rate of roughening) during sliding in the blank holder for cupping operations and smoothing during flat-die friction test sliding are compared. If the model is correct, then the change in roughness as a result of sliding under constant normal pressure can be obtained by subtracting Eq. (3) from Eq. (4) to obtain:

$$\Delta S_q = X_{Slid}\, m_{S_q}^{PX} \quad (6)$$

Plots of roughness change (ΔS_q) versus sliding distance (X_{Slid}) for the cupping operations and the flat-die friction tests should yield identical values of $m_{S_q}^{PX}$. Fig. 12 is a plot of the roughness change as a function of sliding distance for flat-die friction test sliding, interrupted cupping, and full

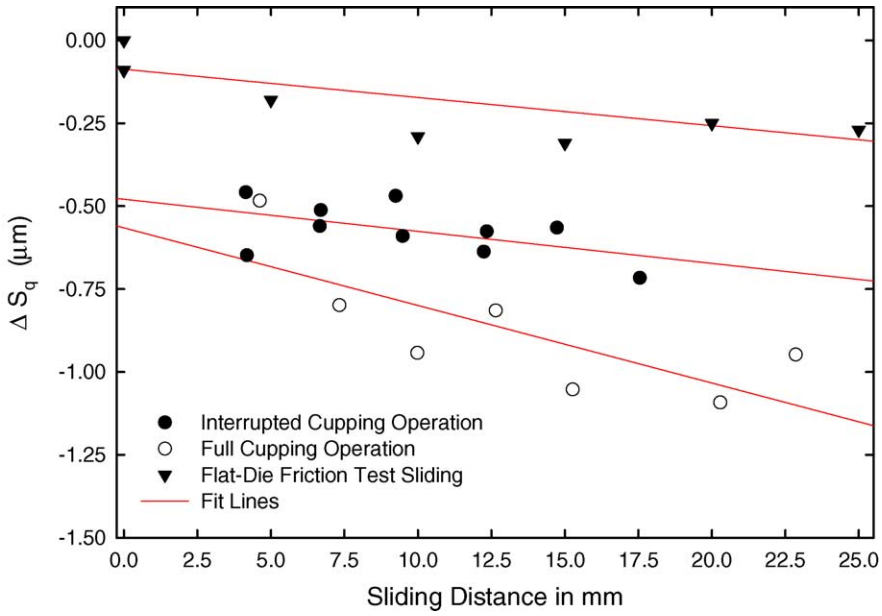

Fig. 12. Change in surface roughness as a function of sliding distance for the interrupted cupping, full cupping and flat die friction test sliding operations.

cupping operations. For flat-die friction test sliding at zero sliding distance, there should be no smoothing due to sliding. The fit line shown in Fig. 12 matches this expectation reasonably well. The slight difference could be the smoothing effect of normal pressure without sliding. In Fig. 12, the smoothing rates, $m_{S_q}^{PX}$, are very similar for the interrupted cupping and the flat-die friction test sliding, however, the interrupted cupping data are offset below the flat-die friction test data. The offset could be a result of differences in lubrication during testing, the applied pressure during testing, or the geometry of the entry points of flat die friction tester versus the geometry of the blank holder. The slope of the lines in Fig. 12 can be used to obtain values of $m_{S_q}^{PX}$ for the friction test and both cupping tests. It can also be used to obtain a value for K_{Bend} for the full cupping test from the intercept of the full cupping test line in Fig. 12. These values are given in Table 2.

The magnitude of $m_{S_q}^{PX}$ for the full cupping operation is much larger than $m_{S_q}^{PX}$ for either the flat-die friction test sliding or the interrupted cupping operation. The best explanation for this is that K_{Bend} is not actually a constant and is increasing in magnitude as the level surface deformation changes before the specimen is bent over the die shoulder. If the effect from sliding is truly independent of the deformation process, $m_{S_q}^{PX}$ for the full cupping operation should be about -9×10^{-3} μm/mm, and K_{Bend} should be some function that increases with increasing strain, sliding distance, or thickness of the sheet.

5.5. Extension of basic equation

This section suggests possible extensions of the model to account for other factors, which affect roughness during a deformation process. Two modifications are proposed to Eq. (5). The first is to account for the dependence of the bending term on the thickness of the sheet, and the second is to account for changes in roughness due to static pressure. Both of these modifications are proposed, although we do not have direct experimental data to verify them.

It is likely that the effect of bending is affected by the thickening of the sheet as it is pulled through the blank holder during cup testing. The gap between the shoulder of the blank holder and the edge of the punch is constant during testing, so any thickening of the sheet during testing would change the local pressure as the sheet moves through this gap. Additionally, a thick material is subject to greater surface strains relative to a thin material when both are bent over the same radius.

The pressure during testing has an effect on roughness during sliding. The clamping force during flat-die friction test sliding was 5 kN. The blank holder force during cupping operations was 12.5 kN. Knowing the contact area of the friction tester allows the calculation of the normal pressure during flat-die testing. However, the pressure distribution over the flange region of the cup and in the die shoulder region was not uniform, thus making pressure calculation difficult, if not impossible. However, if a static normal pressure term – pressure applied without sliding – were introduced into Eq. (5), it could account for the offset between the flat-die friction test results and interrupted cupping test results in Fig. 12. Adding this term to Eq. (5) and the dependence of the bending term on thickness results in an equation that calculates roughening effects based on strain level, sliding distance, pressure during sliding, static pressure, and bending as a function of thickness, t. The equation for surface roughness as a function of deformation mode is:

$$S_q = S_q^0 + \varepsilon_{\text{vme}}\, m_{S_q}^{\varepsilon} + X_{\text{Slid}}\, m_{S_q}^{PX} + P_N^S\, m_{S_q}^{P} + K_{\text{Bend}}(t) \tag{7}$$

6. Conclusions

For the deformation of a hot-dipped galvanized (HDG) zinc-coated sheet steel:

- Surface roughness is a function of both strain level and strain path.
  - Roughness increases with strain, without die contact.
  - Strain path affects roughening rate. Plane strain deformation shows the greatest rate of roughening with respect to strain relative to either drawing or biaxial stretching strain paths.
- Bending and sliding modes of deformation cause a smoothing of the surface.
- Sliding deformation produced during flat-die friction testing causes a decrease in roughness that is identical to that occurring in the interrupted cupping operation.
- It is suggested that the effects of the bending deformation mode on deformation is not constant, but dependent upon thickening of the sheet during prior deformation. It is suggested that the normal pressure during deformation has a smoothing effect on the surface roughness. An equation (Eq. (7)) for the effect of four deformation modes on surface roughness based upon the testing performed in this study has been developed.

Acknowledgements

The authors acknowledge the support for this project by the Advanced Steel Processing and Products Research Center (ASPPRC) at the Colorado School of Mines in Golden, CO, United States of America and Onderzoekscentrum voor aanwending van staal (OCAS) in Zelzate, Belgium. One of the authors (CJVT) thanks the Engineering Research Center for Net Shape and Die Manufacturing (ERC-NSDM) at Busan National University in Korea for the use of their facilities during his sabbatical, which allowed the final writing of this paper.

References

[1] H. Ishigaki, Deformation of large sized panels in the press shop, in: D.P. Koistinen, N.M. Wang (Eds.), Mechanics of Sheet Metal Forming, Plenum Press, New York, NY, USA, 1978, pp. 315–339.
[2] W.F. Hosford, J.L. Duncan, Sheet Metal Forming: A Review, vol. 51 (11), JOM, November 1999, pp. 39–44.
[3] B.M. Hance, R.P. Foley, D.K. Matlock, Effects of Strain Path on Formability and Microstructural Evolution in Low-Carbon Sheet Steels, SAE Technical Paper 970155, SAE, Warrendale, PA, USA, 1997.
[4] W.F. Hosford, R.M. Cadell, Metal Forming Mechanics and Metallurgy, second ed., Prentice Hall, Englewood Cliffs, NJ, USA, 1993.
[5] R. Mahmudi, M. Mehdizadeh, Surface roughening during uniaxial and equi-biaxial stretching of 70-30 brass sheets, J. Mater. Process. Technol. 80–81 (1998) 707–712.
[6] P.F. Thomson, B.V. Shafer, The roughening of free surfaces under deformation, in: Proceedings of the 12th Biennial Congress International Deep Drawing Research Group, Association Italiana di Metallurgia, Milan, Italy, 1982, pp. 123–127.
[7] B. Taylor, Sheet formability testing, Metals Handbook: Mechanical Testing, vol. 8, ninth ed., ASM, Metals Park, OH, USA, 1985, pp. 547–570.
[8] K.J. Stout, P.J. Sullivan, W.P. Dong, E. Mainsah, N. Luo, T. Mathia, H. Zahouani, The Development of Methods for the Characterization of Roughness in Three Dimensions, EUR 15178, ECSC-EEC-EAEC, Brussels-Luxemborg, 1993.
[9] Z. Marciniak, K. Kuczynski, Limit strains in the process of stretch-forming sheet metal, Int. J. Mech. Sci. 9 (1967) 609–620.
[10] C.M. Wichern, B.C. De Cooman, C.J. Van Tyne, Surface roughness changes on a hot-dipped galvanized sheet steel during deformation at low strain levels, Acta Materialia 52 (2004) 1211–1222.
[11] C.M. Wichern, Forming, Surface Topography and Friction Relationships in Zinc-Coated Sheet Steels, Ph.D. Dissertation T-5387, Colorado School of Mines, Golden, CO, USA, 2000.